

Large enhancement of the thermopower in Na_xCoO_2 at high Na doping

Minhyea Lee¹, Liliana Viciu², Lu Li¹, Yayu Wang^{1,†}, M. L. Foo²,

S. Watauchi², R. A. Pascal Jr.², R. J. Cava² and N. P. Ong¹

*Departments of Physics¹ and Chemistry², Princeton University, Princeton, New Jersey 08544, U.S.A.**

(Dated: March 23, 2022)

Research on the oxide perovskites has uncovered electronic properties that are strikingly enhanced compared with those in conventional metals. Examples are the high critical temperatures of the cuprate superconductors and the colossal magnetoresistance in the manganites. The conducting layered cobaltate Na_xCoO_2 displays several interesting electronic phases as x is varied [1, 2, 3], including water-induced superconductivity [4] and an insulating state [3] that is destroyed by field [5]. Initial measurements [1] showed that, in the as-grown composition, Na_xCoO_2 displays moderately large thermopower S and conductivity σ . However, the prospects for thermoelectric cooling applications faded when the figure of merit Z was found to be small at this composition ($0.6 < x < 0.7$). Here we report that, in the poorly-explored high-doping region $x > 0.75$, S undergoes an even steeper enhancement. At the critical doping $x_p \sim 0.85$, Z (at 80 K) reaches values ~ 40 times larger than in the as-grown crystals. We discuss prospects for low-temperature thermoelectric applications.

In the large- x region of Na_xCoO_2 ($x > 0.75$), progress has been hampered by difficulties in growing single crystals as well as by phase-separation effects which appear above x_p . Powder neutron diffraction [6] has revealed subtle shifts in the Na ions as x is increased above 0.75. The doping interval $0.75 < x < x_p$ is a homogeneous phase H_2 , in which the thickness t of the CoO_2 layers undergoes a steep increase [6]. Above x_p , the neutron results indicate phase separation (the mixed-phase region is labelled H_2+H_3). Muon spin rotation [12], nuclear magnetic resonance (NMR) [14] and susceptibility [13, 14] experiments also suggest mixed phases in highly-doped samples. Finally, the limiting phase H_3 ($x \rightarrow 1$) is inferred from NMR and magnetic susceptibility to be a non-magnetic insulator with a slight admixture of a residual metallic phase [13, 14].

In a thermopower experiment, the current density $\mathbf{J}' = \sigma\mathbf{E}$ produced by the E -field is cancelled by the thermoelectric current $\mathbf{J} = \alpha(-\nabla T)$ driven by the applied gradient $-\nabla T$ (α the thermoelectric or Peltier conductivity). Whereas the thermopower $S = \alpha/\sigma$ is the quantity usually reported, we have found that α provides a more incisive probe for sorting out the results in

the region $H_2 + H_3$. Results from 10 crystals (of nominal size $400 \times 700 \mu\text{m}$) with x ranging from 0.71 to ~ 1 reveal that α rises steeply to a peak at the threshold doping x_p , with σ nearly constant (as shown in Fig. 1, samples are labeled 1-10 in order of increasing x). In the mixed region above x_p both quantities decrease rapidly.

Crystals of Na_xCoO_2 grow as either bilayer or tri-layer structures (2 and 3 CoO_2 layers per unit cell, respectively) [9]. The in-plane transport quantities are very similar in the 2 structures. However, at large x , the 3-layer crystals (Samples 2*, 9*, 10*) tend to lock to the commensurate dopings $x = \frac{3}{4}$ and ~ 1 , which provide valuable checks.

Figure 1 displays curves of the observed ρ vs. T (temperature) in the 3-layer (Panel a) and 2-layer (b) cobaltate. Beginning with the lowest curves (Samples 1-4 in Panel b), we note that the profiles of $\rho(T)$ are metallic with the residual resistivity ratio RRR $\simeq 20$, comparable to the as-grown crystals ($0.6 < x < 0.7$). Significantly, in Samples 2*-6 (regions H_2 and slightly beyond x_p), the room-temperature values $\rho(300)$ lie in the range 1-2 $\text{m}\Omega\text{cm}$. As x crosses x_p into $H_2 + H_3$ (Samples 5-8), $\rho(300)$ rises steeply to $\sim 240 \text{ m}\Omega\text{cm}$ (in 10*), which far exceeds the Mott limit. Surprisingly, the curves retain the “metallic” profile even as $x \rightarrow 1^-$. This implies that, for $x > x_p$, the carriers strongly segregate into a fraction f of the layers. The observed $\rho(T)$ reflects the intrinsic resistivity of these conducting layers inflated by the geometric factor $1/f$. Moreover, the persistence of metallic behavior to 4 K implies that the layers remain electrically connected down to low T . Thermal activation of carriers over low barriers, frequently seen in phase-separated systems, is not observed.

Curves of the thermopower are displayed in Fig. 2a. The curve with the smallest S (Sample 1) is typical of as-grown crystals [1, 2]. Across the H_2 region (Samples 2*, 3, 4), the S - T curves show an increasingly negative curvature that grows into a broad peak of magnitude 240 $\mu\text{V}/\text{K}$ at ~ 130 K in 4. In the mixed-phase region, the peak value rises further to 300-350 $\mu\text{V}/\text{K}$ (Samples 5-8), before settling to 200 $\mu\text{V}/\text{K}$ as $x \rightarrow 1$ (Samples 9*, 10*). These large S values far exceed any reasonable extrapolation of the Sommerfeld expression $S = (k_B/e)(k_B T/\epsilon_F)$ (k_B is Boltzmann’s constant and e the electron charge). To match the observed $\partial S/\partial T \simeq 3 \mu\text{V}/\text{K}^2$ at low T , we would need the Fermi energy ϵ_F to equal ~ 30 K, which is unphysically small. The unusually large S , coexisting with low resistivities ($\sim 100 \mu\Omega\text{cm}$ in Samples 4-6), challenges our understanding of how strong correlation enhances the Peltier effect. Approaches include the use

*Nature Materials, *in press*

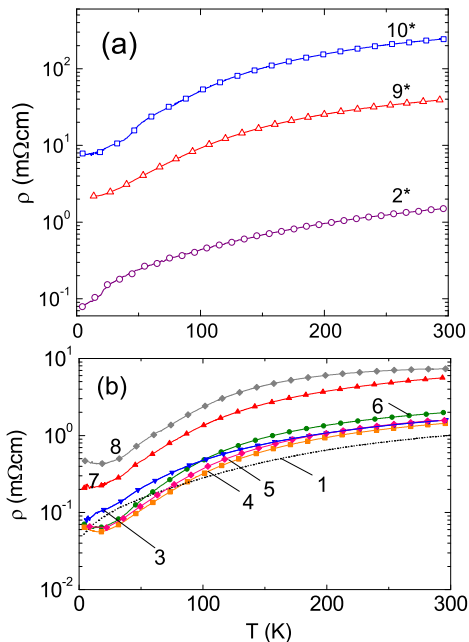


FIG. 1: In-plane resistivity ρ vs. T in the 3-layer (Panel a) and 2-layer (Panel b) cobaltate in log-linear scale. The samples, numbered in order of increasing x , are: Sample 1 ($x \simeq 0.71$), 2* (0.75), 3 (0.80), 4 (0.85), 5 (0.88), 6 (0.89), 7 (0.96), 8 (0.97), 9* (0.99) and 10* (1.0). Asterisks indicate the 3-layer crystals (Panel a). From $x = 0.71$ to $x_p \sim 0.85$, ρ does not change significantly (Samples 1–5). Inside the mixed-phase region $H_2 + H_3$, however, ρ increases rapidly (6–10*). The persistent metallic profile inside $H_2 + H_3$ suggests that conducting layers are embedded in an insulating matrix. Scaling of the curves of ρ are not as satisfactory as for α (see below). Contacts with contact-resistance 2–10 Ω were attached by lightly abrading the crystal surface and attaching Au wires with Ag paint (Du Pont 4922N). The size of contact pads (see Supplement) leads to a total uncertainty in the absolute values of ρ of $\pm 15\%$.

of the Heikes formula [2, 15, 16].

In Fig. 2b, we display plots of the figure of merit $Z = S^2/\rho\kappa$ for some of the samples (κ is reported in Supplementary Information). Near the threshold x_p (Samples 4, 5), Z rises to a prominent maximum below 100 K. As mentioned, the peak value of Z at 80 K is ~ 40 times larger than that in the as-grown composition (compare 5 with 1). We discuss Z below. The dimensionless figure of merit ZT is plotted in Supplementary Information.

The Peltier conductivity α shows nominally similar profiles (Fig. 3a). In Samples 1 and 2*, α displays broad peaks at 100 and 80 K, respectively, but remains fairly small. As we enter the H_2 region, however, α increases rapidly, displaying a sharply peaked profile in Sample 4. In simple metals, $\alpha \sim (k_B^2/e)(T/\epsilon_F)\sigma$ decreases linearly to zero as $T \rightarrow 0$. At high T , α tends to saturate to values in the range 1–10 A/mK. Hence, the pronounced peak and large values of α reported here ($\alpha_{max} \sim 135$

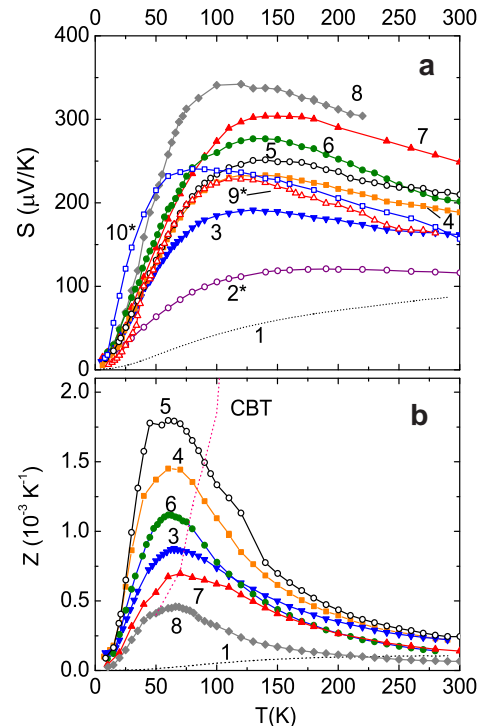


FIG. 2: The in-plane thermopower S (Panel a) and the figure of merit Z (Panel b) in Na_xCoO_2 . In Sample 1 (Panel a), S is very similar to that of Terasaki *et al.* [1]. As x increases into phase H_2 (2*–4), the profile of S develops an increasing bulge near 130 K that grows rapidly to peak values of 200–250 $\mu\text{V/K}$. In the mixed-phase region, S further increases to 300–350 $\mu\text{V/K}$ (Samples 5–8), before settling down to 228 $\mu\text{V/K}$ in the limit $x \rightarrow 1$ (Samples 9*). A striking pattern is that the S - T profiles (all hole-type) are nominally similar in shape in the mixed-phase region. The exception is Sample 10* in which $f \sim 1/200$ (see Supplementary Information). Panel b shows curves of $Z = S^2/\rho\kappa$, with κ measured separately (not shown). As x increases from 0.71 (Sample 1), the peak value of Z increases steeply to $1.8 \times 10^{-3} \text{ K}^{-1}$ in Sample 5. At higher x , the peak value of Z falls rapidly because of the sharp increase in ρ . At 80 K, Z in Sample 5 is ~ 40 times larger than that in Sample 1. The dashed line labeled CBT is Z reported [17] for CsBi_4Te_6 .

A/mK in Sample 4) are strikingly anomalous, and likely a consequence of strong correlation.

By tracking T_{max} (the peak temperature of α), we see that α vs. T in 1–4 ($x \leq x_p$) evolves differently from α in 5–10* (in $H_2 + H_3$). In the first group, T_{max} decreases from 110 K to 50 K (in 1 and 4, respectively). The continuous change in T_{max} precludes a simple scaling analysis. By contrast, in the second group, T_{max} remains fixed at ~ 50 K. Moreover, by multiplying each curve by a scale factor p , we may match it to the curve of 4 (Fig. 3b). The exception is Sample 6 which has a cusp at 36 K (of unknown origin) that ruins the scaling. Hence, as we traverse the homogeneous region H_2 , the peak value of

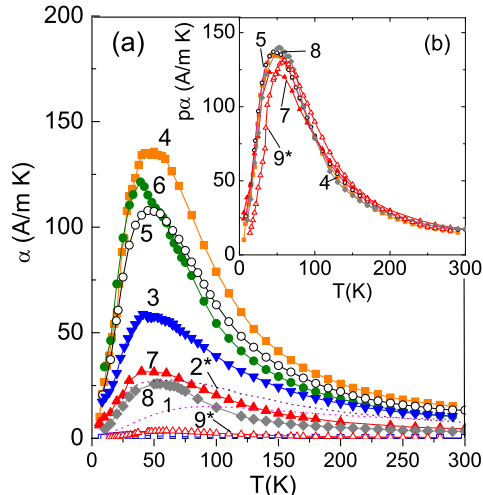


FIG. 3: Curves of the Peltier conductivity α vs. T (Panel a) and scaling of the α - T curves in selected samples (Panel b). As x traverses the region H_2 (Samples 1–4) the peak in $\alpha(T)$ systematically shifts from 100 K to 50 K. Because of the shift these curves cannot be scaled together. However, in the region $H_2 + H_3$ (5–10), the peak in α remains at 50 K. Panel b shows that the curves of 5–10 match the template in 4 when multiplied by the scale factor p ($p = 1.3, 3.9, 5.4, 38$ and 200 in Samples 5, 7, 8, 9^* , and 10^* , respectively). Sample 6 has a cusp of unknown origin that makes it an exception. Sample 10^* is discussed in Supplement.

α increases rapidly from 20 A/mK in 2^* to 135 A/mK in 4, but the form of α vs. T also changes continuously. However, once we cross the threshold x_p into the mixed phase, the profile is locked to that of 4.

The simplest explanation of the scaling is that, in $H_2 + H_3$, the carriers segregate into *continuous* conducting layers embedded in a nearly insulating matrix. The conducting layers correspond to doping x_p whereas the insulating matrix is at $x = 1.0$. The mean doping x_m is then given by

$$x_m = f x_p + (1 - f), \quad (x_p < x_m < 1) \quad (1)$$

where f is the fraction of layers with doping x_p . Additivity of the Peltier currents implies that the observed α is given by

$$\alpha(T) = f \alpha_p(T) + (1 - f) \alpha_1(T), \quad (2)$$

where subscripts p and 1 refer to quantities evaluated at $x = x_p$ and 1, respectively.

The scaling behavior in Fig. 3b implies that the second term in Eq. 2 is negligible if f is not too small. The Peltier conductivity $\alpha_1(T)$, which has a maximum value of ~ 0.85 A/mK, is observable only when f becomes very small, as in the case of Sample 10^* (see Supplementary Information). Away from this limit, we may take $f \simeq 1/p$ throughout the mixed-phase region; this allows us to find

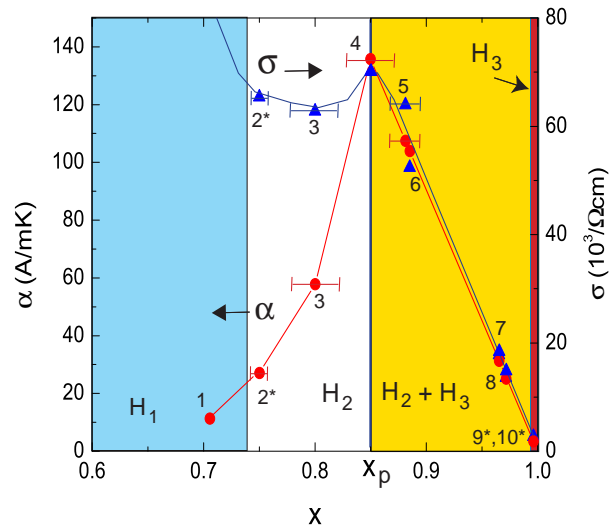


FIG. 4: Variation of α (50 K) and σ (300 K) vs. x in Na_xCoO_2 at large x (Sample labels shown). As x traverses H_2 , $\alpha(50)$ rises sharply to a maximum at x_p in correlation with the increase in the CoO_2 layer-thickness t [6]. Because $\sigma(300)$ is nearly constant, the peak in $\alpha(50)$ leads to a peak in Z as well. In $H_2 + H_3$, α and σ (plotted vs. x_m calculated from p using Eq. 1) decrease linearly as $x_m \rightarrow 1^-$, implying phase-separation of holes into conducting layers. The phase H_3 is insulating. In the trilayer crystals (2^* , 9^* , 10^*) x is locked to the commensurate values $\frac{3}{4}$ and ~ 1 . The x values in Samples 1 and 4 were measured by x-ray diffraction (lines are guides to the eye). Error bars in x_m reflect the uncertainty in measuring ρ and S (see Supplementary Information).

x_m using Eq. 1. For e.g., in Sample 9^* , the scaling of α shows that 1 in 40 of the layers is conducting ($x_m = 0.996$ instead of 1.00), which is consistent with the observed $\rho(300)$ in Fig. 1a. In addition, we have employed other checks on the calibration. The trilayer crystals, with $x = \frac{3}{4}$ and ~ 1 , provide valuable calibration points. Moreover, x in Samples 1 and 4 was determined from the c -axis lattice parameter measured by x-ray diffraction. These checks lend support for our calibration.

With the inferred values of x and x_m , we next plot the variation of α at 50 K (circles) and σ (triangles) at 300 K in the phase diagram at large doping (Fig. 4). From $x = 0.71$ to x_p , $\alpha(50)$ rises by a factor of 14. The modest changes in $\sigma(300)$ (triangles) and κ (see Supplementary Information) result in a substantial increase in Z . We emphasize that these increases occur within the homogeneous phase H_2 and are possibly correlated with the increase in layer thickness t [6]. Clearly, they are not a consequence of the phase separation that onsets at x_p . Both quantities decrease linearly above x_p .

The 40-fold enhancement of Z realized at 80 K improves greatly the prospects for thermoelectric applications. The peak value in Fig. 2b ($Z \sim 1.8 \times 10^{-3} \text{ K}^{-1}$) is among the highest known for a *hole*-type material below 100 K. The promising material CsBi_4Te_6 also displays a large Z at 100 K [17]. In comparison, Z in

Na_xCoO_2 peaks at low temperatures whereas the curve for CsBi_4Te_6 (curve labeled CBT) falls steeply. The alloy $\text{Bi}_{1-y}\text{Sb}_y$ has long been known [18] to display an even larger Z at low T (at 80 K, $Z = 7 \times 10^{-3} \text{ K}^{-1}$ for $y \sim 0.12$). However, it is electron-like. To realize its advantages in a Peltier device operating below 100 K, we need to pair Bi-Sb with a hole-type material with comparable Z , but the 35-year search has turned up no viable candidates. We calculate that an optimized device with Na_xCoO_2 ($x = x_p$) paired with $\text{Bi}_{1-y}\text{Sb}_y$ has a device figure-of-merit $Z_{np} = 2.5 \times 10^{-3} \text{ K}^{-1}$ at 80 K [$Z_{np} = (S_n - S_p)^2 (\sqrt{\rho_n \kappa_n} + \sqrt{\rho_p \kappa_p})^{-2}$ where subscripts n and p index the 2 materials]. This value is higher than any reported to date. Further enhancement of Z in Na_xCoO_2 seems possible if we degrade κ .

Methods

Sodium metal (0.5 g) and tetrahydrofuran (THF) (30

mL) in a pyrex tube were warmed at 100 °C in an oil bath [6]. Benzophenone (2 g) was added and the solution heated until it turned blue from the formation of the benzophenone ketyl radical anion. As-grown crystals of $\text{Na}_{0.75}\text{CoO}_2$ were placed along a pipette-like tube and immersed in the blue solution of the sodium radical anions. The pyrex tube was quickly capped and heated for 4 days at 100 °C. Finally, the crystals were extracted and washed with THF and ethanol to eliminate trace sodium.

This research is supported by the U.S. ONR (Contract N00014-04-1-0057) and by NSF Grant DMR 0213706.

Correspondence and requests for materials should be addressed to NPO (np0@princeton.edu).

Supplementary information posted online.

[†]Current address of Y.W.: Department of Physics, Univ. California, Berkeley, CA 94720.

-
- [1] Terasaki, I., Sasago, Y. & Uchinokura, K., Large thermoelectric power in NaCo_2O_4 single crystals. *Phys. Rev. B* **56** R12685 -R12687 (1997).
- [2] Wang, Y., Rogado, N. S., Cava, R. J., & Ong, N. P., Spin entropy as the likely source of enhanced thermopower in $\text{Na}_x\text{Co}_2\text{O}_4$ *Nature* **423**, 425-428 (2003).
- [3] Foo, M. L. *et al.*, Charge Ordering, Commensurability, and Metallicity in the Phase Diagram of the Layered Na_xCoO_2 . *Phys. Rev. Lett.* **92**, 247001 (2004).
- [4] Tanaka, K. *et al.*, Superconductivity in two-dimensional CoO_2 layers. *Nature* **422**, 53 - 55 (2003);
- [5] Balicas, L., Abdel-Jawad, M., Hussey, N. E., Chou, F. C., & Lee, P. A., Shubnikov de Haas Oscillations and the Magnetic-Field-Induced Suppression of the Charge Ordered State in $\text{Na}_{0.5}\text{CoO}_2$. *Phys. Rev. Lett.* **94**, 236402 (2005).
- [6] Huang, Q. *et al.* Coupling between electronic and structural degrees of freedom in the triangular lattice conductor Na_xCoO_2 . *Phys. Rev. B* **70**, 184110 (2004).
- [7] Bayrakci, S. P. *et al.*, Bulk antiferromagnetism in $\text{Na}_{0.82}\text{CoO}_2$ single crystals. *Phys. Rev. B* **69** 100410(R) (2004).
- [8] Bayrakci, S. P. *et al.*, Magnetic Ordering and Spin Waves in $\text{Na}_{0.82}\text{CoO}_2$. *Phys. Rev. Lett* **94** 157205 (2005).
- [9] Viciu, L. *et al* Crystal Structure and Elementary Properties of Na_xCoO_2 ($x = 0.32, 0.5, 0.6, 0.75,$ and 0.92) in the Three-Layer NaCoO_2 Family, cond-mat/0601587.
- [10] Bernhard, C. *et al.* Charge Ordering and Magnetopolarons in $\text{Na}_{0.82}\text{CoO}_2$. *Phys. Rev. Lett* **93** 167003 (2004).
- [11] Sugiyama, J. *et al.*, *Phys. Rev. Lett* **92** 017602 (2005).
- [12] Mendels, P. *et al.* Cascade of Bulk Magnetic Phase Transitions in Na_xCoO_2 as Studied by Muon Spin Rotation *Phys. Rev. Lett* **94** 136403 (2005).
- [13] Lang, G. *et al.* Evidence of a single nonmagnetic Co^{3+} state in the Na_1CoO_2 cobaltate. *Phys. Rev. B* **72**, 094404 (2005).
- [14] de Vaulx, C. *et al.* Nonmagnetic Insulator State in Na_1CoO_2 and Phase Separation of Na Vacancies. *Phys. Rev. Lett* **95**, 186405 (2005).
- [15] Koshibae, W. & Maekawa, S. Effects of spin and orbital degeneracy on the thermopower of strongly correlated systems, *Phys. Rev. Lett.* **87**, 236603 (2001).
- [16] Chaikin, P.M. & Beni, G. Thermopower in the correlated hopping regime. *Phys. Rev. B* **13**, 647-651 (1976).
- [17] D.-Y. Chung *et al.*, CsBi_4Te_6 : A high-performance thermoelectric material for low-temperature applications. *Science* **287**, 1024-1027 (2000).
- [18] Yim, W. M. & Amith, A., Bi-Sb alloys for magnetothermoelectric and thermomagnetic cooling, *Solid-State Electronics* **15**, 1141-1165 (1972).

Supplementary Information

Breakdown of scaling in Sample 10*

We provide more details on the measurements and analysis of the thermopower S and resistivity ρ in the phase-separated region $H_2 + H_3$, especially in the extreme case $x \rightarrow 1^-$ represented by Sample 10*.

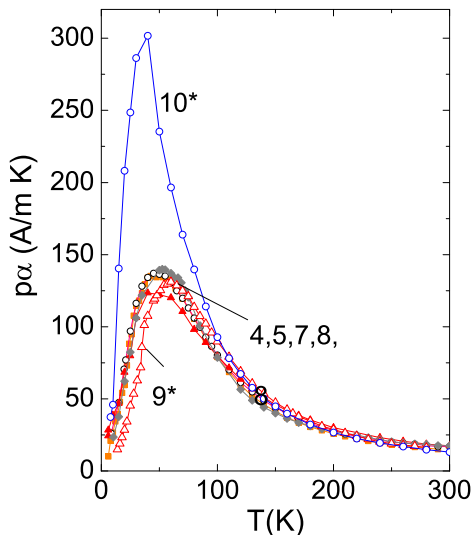


FIG. 1: Comparison of the scaled curves of $p\alpha(T)$ in Sample 10* with those in the batch Samples 4–9* (the scale factor $p = 200$ in Sample 10*). Above 100 K, the scaled curve matches those in 4–9*. Below 100 K, the additional contribution which we identify with α_1 in the $x = 1$ phase becomes prominent. The peak value of α_1 is 0.85 A/mK. This additional term causes the thermopower $S(T)$ in 10* to be distinct in profile from Samples 4–9* (see Fig. 2a of the text).

As noted in the text, the simplest interpretation of the scaling behavior in the curves of the Peltier conductivity α vs. T is to assume that the hole carriers strongly segregate into parallel layers throughout each crystal. The layers must remain robustly connected electrically even at 4 K (otherwise we would not have the metallic profile in ρ with the large residual resistivity ratios $\text{RRR} \sim 20$). Additivity of the currents implies that the observed α and σ are given by

$$\alpha(T) = f\alpha_p(T) + (1-f)\alpha_1(T), \quad (3)$$

$$\sigma(T) = f\sigma_p(T) + (1-f)\sigma_1(T), \quad (4)$$

where subscripts p and 1 refer to quantities evaluated at $x = x_p$ and 1, respectively.

The similarity of the ρ - T profiles in Fig. 1 of the text implies that all of \mathbf{J} is carried by the conducting layers. Setting $\sigma_1 = 0$, we have for the observed thermopower

$$S(T) = S_p(T) + \frac{(1-f)\alpha_1(T)}{f\sigma_p(T)}, \quad (5)$$

with $S_p = \alpha_p/\sigma_p$.

In Samples 5–9*, in which the curves of α vs. T may be scaled to that in Sample 4, the term $(1-f)\alpha_1$ must be negligible compared with $f\alpha_{x_p}$ in Eq. 3 (Sample 6 is excluded). Further, if the second term in Eq. 5 is negligible (i.e. $f > 0.05$), all the profiles of $S(T)$ should be identical to S_p (Sample 4). We find that, apart from a 20% spread in magnitude, the curves of $S(T)$ are indeed closely similar in Samples 4–9*.

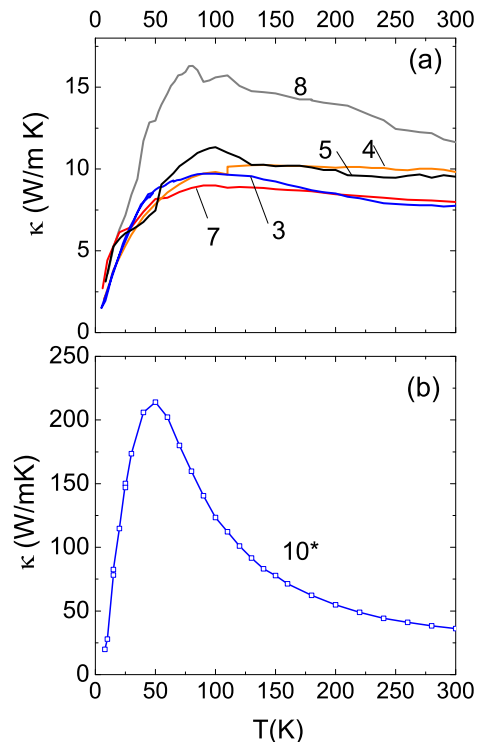


FIG. 2: Curves of the in-plane thermal conductivity κ vs. T in Samples 3–8 of Na_xCoO_2 (Panel a) and in Sample 10* (Panel b). The magnitude of $\kappa = 8$ –10 W/mK above 50 K in Samples 3–7 is characteristic of doped layered perovskites. In Sample 10* ($x \simeq 1$), κ attains much larger values, possibly reflecting the pristine nature of the Na ordering. It is of the same order as crystals in the charge-ordered insulating state ($x = 0.5$).

This spread reflects difficulties in establishing the absolute values of S and ρ accurately. The size of the contact pads (50–100 μm) relative to that of the crystals (400–700 μm on a side) leads to uncertainties of $\pm 10\%$ in estimating the voltage lead separation. This is exacerbated by the large electrical anisotropy ρ_c/ρ where ρ_c is the c -axis resistivity, which causes a small admixture of ρ_c into the measured “in-plane” resistance despite deliberate care at optimal contact pad placement. We suspect that the latter factor is the main factor that spoils exact scaling of the ρ - T profiles. Altogether, we estimate a combined uncertainty of $\pm 15\%$ in the absolute values of

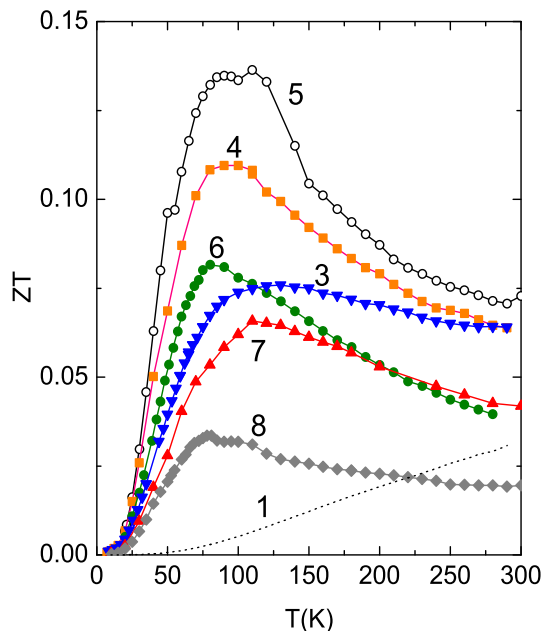


FIG. 3: Plots of the dimensionless figure-of-merit ZT in Samples 1-8 (except 2).

ρ . Within this uncertainty, we see that, in Samples 4–9*, the profiles of S vs. T remain strikingly similar despite the 50-fold increase in ρ in these samples.

The prominent exception is Sample 10*. As shown in Fig. 1, the scaled curve $p\alpha(T)$ matches those in the other samples above 100 K. The value of the scale factor $p \sim 200$ inferred from this plot is also consistent with the resistivity data ($\rho(300)$ in Sample 10* ~ 240 m Ω cm nominally equals $\rho(300)$ in Sample 4 multiplied by p). Below 100 K, however, a further contribution, which we identify with $\alpha_1(T)$ in Eq. 3, becomes dominant. We note that the actual peak value of α_1 is ~ 0.85 A/mK, which is unresolvable in Fig. 3a of the text. While this is a very small value, it can make the second term in Eq.

3 comparable to the first if f becomes very small. This is the case in Sample 10* near 50 K, for which $f\alpha_p \sim 0.68$ A/mK. Hence, in this extreme limit, we estimate that 1 in 200 of the layers carries the applied current to produce a “metallic” resistivity profile resembling that in Sample 4 (apart from the scale factor). In principle, the observed thermopower and α should also match that of 4. However, in Sample 10*, the term in α_1 dominates that of the conducting layers below 100 K and ruins the scaling behavior.

Thermal conductivity

For completeness, we show the in-plane thermal conductivity measured in some of the samples in Fig. S2. These curves were used in computing the figure of merit $Z = S^2/\rho\kappa$, with κ the in-plane thermal conductivity. Throughout the region H_2 , κ has the modest value 10 W/mK, quite typical of layered perovskites (Fig. S2a). However, in the limit $x = 1$, κ becomes very large (Fig. S2b), attaining values in the charge-ordered state¹ at $x = 0.5$.

Dimensionless Figure of Merit ZT

Some authors prefer to use the dimensionless figure-of-merit ZT in place of Z . For comparison, we have replotted the curves of Z vs. T in Fig. 2b of the text as ZT vs T in Fig. S3. An interesting feature of these curves is that ZT attains a prominent maximum at temperatures between 60 and 100 K in the layered cobaltate. By comparison, in high-performance thermoelectric materials based on doped Bi_2Te_3 the maximum in ZT occurs in the interval 200–300 K (see for e.g. Chung *et al.*²). The rapid fall of ZT in the Bi_2Te_3 family reflects the semi-metallic nature of the bands. In the cobaltates, however, the peaking of ZT at much lower T is a consequence of the very narrow bands and the magnetic correlations that are present because of strong interaction between carriers.

References

1. Foo, M. L. *et al.*, Phys. Rev. Lett. **92**, 247001 (2004).
2. D.-Y. Chung *et al.*, Science **287**, 1024-1027 (2000).